Zero-temperature spin dynamics of a random two-dimensional XY model

P. Gawiec and D. R. Grempel
Laboratoire de Magnétisme et Diffraction Neutronique, DRFMC/SPSMS, Centre d'Etudes Nucléaires de Grenoble, 85X, F-38041 Grenoble Cedex, France

(Received 25 February 1993; revised manuscript received 3 May 1993)

We study the zero-temperature spin dynamics of a random-exchange two-dimensional XY model using both exact numerical methods and an approach based upon the coherent potential approximation (CPA). The model, which presents a mixed-phase to spin-glass phase transition, consists of a ferromagnetic host with nearest-neighbor bonds J to which one substitutes impurity bonds of strength $-\lambda J$ at concentration x. In both phases, the long-wavelength magnetic excitations of this system are spin waves with a linear spectrum. The x and λ dependence of the spin-wave velocity is determined numerically by calculating the stiffness constant of the system with a new transfer-matrix algorithm. The stiffness constant and the spin-wave velocity decrease rapidly with increasing x. The two quantities are smooth across the phase boundary, and they saturate in the spin-glass phase. At shorter wavelengths, the q dependence of the energies and lifetimes of the spin waves in the ferromagnetic and spin-glass states differs qualitatively, reflecting the morphological differences that exist between the spin configurations characteristic of the two phases. Line shapes and linewidths depend strongly on the polarization of the excitations. Whereas out-of-plane modes stay propagative at all concentrations, in-plane ones are inhomogeneously broadened and are overdamped at long wavelengths. There is good overall agreement between the exact numerical results and those obtained using the CPA.

I. INTRODUCTION

The layered high-T_c superconductors $YBa_2Cu_3O_{6+\delta}$ and $La_{2-\delta}Sr_\delta Cu_2O_4$ as well as related materials exhibit an interesting magnetic phase diagram in their insulating phase. At low temperature, the stoichiometric compounds ($\delta=0$) are easy-plane antiferromagnets. The exchange interaction, very strong within the magnetic CuO_2 layers, is weak between them and, hence, the spin-spin correlations are quite accurately two dimensional (2D). It is very well established experimentally[1] that the magnetic properties of the pure compounds are well described in terms of the nearest-neighbor 2D Heisenberg model.[2] Long-range antiferromagnetic order is rapidly lost upon doping and, at a critical value δ_c, the system enters a spin-glass phase. This transition is accompanied by important modifications of the spin dynamics that include a strong q-dependent renormalization of the spin-wave energies and by changes of the line shape that depend upon the polarization of the magnetic excitations.[3,4]

The strong sensitivity of the magnetic properties of the cuprates to δ was explained by Aharony *et al.*[5] who showed that, in the nonstoichiometric compounds, magnetic frustration effects lead first to a lowering of the Néel temperature and subsequently to the disappearance of long-range magnetic order. Such effects arise because, upon doping, in the insulating phase localized electronic holes appear on a fraction of the O^{2-} ions in the CuO_2 planes transforming them into O^- ions. Since the sign of the exchange interaction between two Cu spins is either negative or positive according to whether the oxygen site between them is occupied by an O^{2-} or an O^- ion, this mechanism leads to a model for the doped magnetic planes in which as many of the antiferromagnetic bonds of the original Heisenberg Hamiltonian as there are holes on the CuO_2 plane are substituted by ferromagnetic ones.[5,6]

The static[7-9] and dynamical[10-16] properties of spin models with competing interactions have recently been treated by a number of authors. In some of this work, analytical and numerical methods are used to study the effect on the local magnetic order of a small concentration of magnetic defects, such as vacancies[15] or isolated bonds of the wrong sign.[12-14] The structure factor of a model where the impurity bonds are uniformly distributed has been recently discussed by Saslow and Erwin.[16] Closer to the spirit of this work, Ching and Huber[10,11] have numerically determined the dynamic structure factor of a disordered isotropic Heisenberg antiferromagnet and applied their results to a description of the crossover between the antiferromagnetic and spin-glass states in $La_{2-\delta}Sr_\delta Cu_2O_4$.

In this paper we present numerical and analytical results for the spin-wave dynamics of a disordered XY model with a Hamiltonian

$$H=-\sum_{\langle i,j\rangle} J_{i,j}(S_i^x S_j^x+S_i^y S_j^y)\ . \tag{1}$$

Here, the exchange integrals J_{ij} are random variables with two possible values, J, with probability $(1-x)$ and $-\lambda J$, with probability x. Some comments are in order on the choice of the Hamiltonian and its relationship to the systems studied experimentally. A difference between the model in Eq. (1) and the cuprates is that, in the latter, the exchange is only weakly anisotropic, whereas the former describes a system with large [O(1)] anisotropy. In the

0163-1829/93/48(10)/7114(11)/$06.00

compounds of interest, the average magnetic moments lie on a plane even in the presence of strong disorder.[3,17] This fact determines many of the features of the observed excitation spectrum, in particular, its dependence on spin polarization that we wish to reproduce. In an isotropic or weakly anisotropic model, a general impurity configuration will result in a sizable fraction of the spins coming out of the plane, at least for large values of λ. We thus decided to put the z component of the exchange equal to zero as a simple device to force the ground state to be planar whatever the strength of the disorder. It is clear that the spin dynamics of the model and the real systems is qualitatively similar. Contrary to the cuprates, the impurities in the model are *antiferromagnetic* bonds in a *ferromagnetic* host. This difference is only apparent since the two systems are, in fact, equivalent. This can be seen by performing a unitary transformation of Eq. (1) consisting of a rotation of all the spins on one of the sublattices of the 2D square lattice by an angle π around the z axis. This equivalence, exact in the planar model, holds only in the classical limit in the case of a system with isotropic exchange. Finally, although the ratio of the ferro- to antiferromagnetic couplings, λ, is fixed (and large), for the cuprates it is of interest to treat it as a free parameter and study the dependence of physical quantities in the x-λ plane. In a previous paper,[7] we reported a detailed investigation of the ground-state properties of model (1) in the classical limit. The resulting $T=0$ phase diagram is shown in Fig. 1. Depending upon the values of x and λ, the ground state of the system is either an isotropic spin glass or a mixed phase where a finite magnetization and transverse spin-glass ordering coexist. These two phases are separated by a second-order transition line $x_c(\lambda)$. In this work, we study the spin-wave dynamics of the model in these two different regions of the phase diagram.

The paper is organized as follows. In Sec. II, we discuss the long-wavelength end of the excitation spectrum where the magnetic excitations are long-lived spin waves with a linear energy-momentum relationship. The spin-wave velocity, c, is determined by two macroscopic parameters, the stiffness constant, ρ, and the perpendicular susceptibility, $\chi_\perp$, that we study as a function of x and λ. We have developed an approach for the calculation of the stiffness constant in which a twist is first imposed on the sample by introducing site-dependent Lagrange multipliers into the Hamiltonian and then, the change of the ground-state energy, related to ρ, is determined by a transfer-matrix method. This approach turns out to be far more efficient than traditional ones[18] and makes it possible to calculate numerically the stiffness constant for very large systems. The main conclusion of this section is that ρ and c are analytic functions of x, that are finite everywhere except in the percolation region $\lambda=0$, $x \geq \frac{1}{2}$. This is a necessary condition for the existence of hydrodynamic spin waves.[19] This behavior differs from that of the defect energy, E_d, studied by other authors,[20,21] that vanishes at the boundary between the mixed and spin-glass phases.

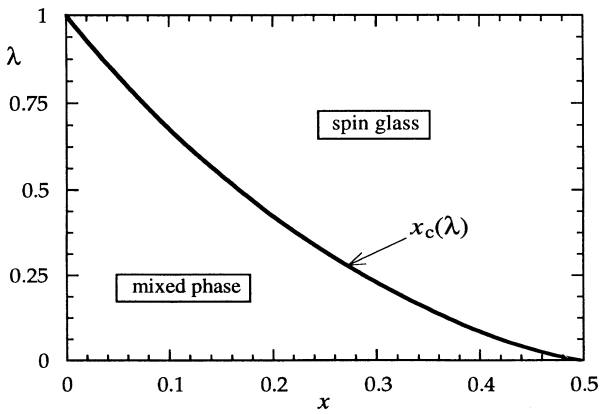

FIG. 1. Zero-temperature phase diagram of the random-exchange XY model.

In Sec. III, we study the spin-wave spectrum in the whole $\mathbf{q}$-ω plane by direct diagonalization of the dynamical matrix following the method developed by Walker and Walstedt[22,23] and Huber and Ching[24,25] for the isotropic model. We find that there exist important differences between the q dependence of the energies and widths of the magnetic excitations in the spin-glass and mixed phases due to the existence in the latter of large ordered regions within which short-wavelength spin-waves propagate almost freely. There is some universal behavior in the spin-glass phase in the sense that, within the accuracy of our calculations, the width of the excitations depends upon the disorder only through the dependence upon the latter of the excitation energy. The theoretical line shapes depend on the polarization of the excitations: whereas out-of-plane excitations are propagative regardless of the strength of the disorder, in-plane modes are inhomogeneously broadened and their line shape is diffusive at long wavelengths.[26]

In Sec. IV, we determine the dynamic structure factor within an approach based on a generalized form of the coherent potential approximation (CPA), appropriate for the case of the XY model. Application of the CPA is much more involved in the latter case than in that of the isotropic model[27–29] due to the lowering of symmetry. The results of this approximation are in very good agreement with the exact ones, showing that the CPA is a good alternative to the heavy numerical calculations described in the first two parts. Section V is devoted to our conclusions.

II. LONG-WAVELENGTH SPIN WAVES

The first step in the analysis of the Hamiltonian of Eq. (1) is the discussion of the ground state in the classical limit, $S \to \infty$. In this limit, the relevant states of the system are determined by the stationary points of the energy functional:

$$H_{\text{class}} = -S^2 \sum_{\langle ij \rangle} J_{ij} \cos(\theta_i - \theta_j) \ . \tag{2}$$

In the systems that interest us, the ground state is not unique but it consists of a large number of almost degenerate spin configurations of different morphology.[7–9,30,31] Spin-wave expansions can be performed around each of these configurations as described in the next section, and

physical quantities, such as correlation functions, may be computed by averaging the results over the elements of the ground-state manifold.

In the long-wavelength limit, $\mathbf{q}$ and $\omega \to 0$, the spin dynamics is particularly simple. By general arguments, the magnetic excitations in this limit should be long-lived spin waves with a linear spectrum, $\omega(\mathbf{q})=c|\mathbf{q}|$, $c^2=\rho/\chi_\perp$.[19,32] The spin-wave velocity c is determined by two thermodynamic quantities, the stiffness constant ρ, and the perpendicular susceptibility $\chi_\perp$, whose dependence upon disorder we wish to study.

The transverse susceptibility $\chi_\perp$ is the linear response of the system to a uniform magnetic field applied in the direction perpendicular to the XY plane. Its computation is elementary. One must generalize Eq. (2) to allow small excursions of the spins out of the plane, and to include the coupling to a magnetic field in the perpendicular direction in the Hamiltonian. Computation of the free energy up to second order in the magnetic field yields

$$\chi_\perp=\frac{1}{SN_s}\sum_i \frac{1}{\lambda_i}, \quad \lambda_i=\sum_j J_{i,j}\cos(\theta_i^0-\theta_j^0) , \tag{3}$$

where we have defined the local fields λ_i.

The stiffness constant, the response of the system to a twist in the boundary conditions, is more difficult to calculate. Let us denote by $\{\theta_i^0\}$ one of the ground-state configurations of a system of $N\times N$ spins with periodic boundary conditions along the x and y directions, and by $\{\theta_i^1\}$ the state into which the first one evolves upon application of an infinitesimal twist φ along the x direction (say). Then, the stiffness constant ρ is defined by

$$\{E[\theta_i^1]-E[\theta_i^0]\}_{\rm av}\equiv\tfrac{1}{2}\rho\varphi^2+O(\varphi^4) . \tag{4}$$

The average in Eq. (4) is over all the configurations in the ground state. A straightforward procedure to determine the stiffness constant is to start from an energy minimum, $\{\theta_i^0\}$, to impose a small but *finite* twist and then to find a new extremum by reminimization of the energy by an iterative method in which $\{\theta_i^0\}$ is taken as the initial condition.[18] However, this procedure is inapplicable to the case at hand for the following reason. An essential point in the definition of ρ is that $\{\theta_i^1\}$ and $\{\theta_i^0\}$ represent the *same* minimum of the energy, the former configuration being a smooth distortion of the latter, resulting from the application of an *infinitesimal* twist. Since in our ground-state manifold the energies of morphologically different configurations differ by tiny amounts, there is no way to assure that the reminimization of the energy in the presence of a *finite* twist leads to the required state rather than to one that is unrelated to the latter. If that was the case, the energy difference between the two states would reflect the structure of the ground state rather than the stiffness of the system. In the following we shall describe a method that we have found that allows us to circumvent this difficulty.

Application of twist boundary conditions to a disordered system results in the appearance of an inhomogeneous internal distortion, $\psi_i=\theta_i^1-\theta_i^0$. For an infinitesimal twist, the energy difference of Eq. (2) may be expanded up to second order in ψ_i:

$$E[\theta_i^1]-E[\theta_i^0]=\tfrac{1}{2}S^2\sum_{i,j}\psi_i M_{ij}\psi_j+O(\psi^4) , \tag{5a}$$

where

$$M_{ij}=\sum_k J_{ik}\cos(\theta_i^0-\theta_k^0)\delta_{ij}-J_{ij}\cos(\theta_i^0-\theta_j^0) . \tag{5b}$$

The site-dependent distortion ψ_i may be determined by minimizing Eq. (4) subject to the twist boundary conditions. Thinking of the system as consisting of $(N+1)$ columns and N rows of spins, the latter may be written in the form $\psi_m^{N+1}-\psi_m^1=\varphi$ where the index m runs on the rows. These constraints can be handled by introducing Lagrange multipliers μ_m, and Legendre-transforming Eq. (4) to obtain the modified energy functional F:

$$F=\tfrac{1}{2}S^2\sum_{n,n'}\sum_{m,m'}\psi_m^n M_{m,m'}^{n,n'}\psi_{m'}^{n'}-\sum_m \mu_m(\psi_m^{N+1}-\psi_m^1-\varphi) , \tag{6}$$

where the upper and lower indices represent the columns and the rows, respectively. Minimizing Eq. (6) with respect to the angles and to the Lagrange multipliers, and eliminating the latter in favor of the twist angle φ, we arrive after some algebra at

$$F_{\min}=\tfrac{1}{2}\varphi^2 S^2\sum_{m,m'}(K^{-1})_{m,m'}\equiv\tfrac{1}{2}\rho\varphi^2 , \tag{7}$$

which gives an expression for ρ in terms of the elements of the matrix $\mathbf{K}$:

$$K_{m,m'}=G_{m,m'}^{N+1,N+1}-G_{m,m'}^{N+1,1}+G_{m,m'}^{1,1}-G_{m,m'}^{1,N+1} , \tag{8}$$

where G denotes the inverse of M.

Straightforward inversion of the $N_s\times N_s$ matrix M is an operation that requires $\sim N_s^3$ computational steps. Thus, it becomes rapidly prohibitively time consuming when the number of spins, N_s, increases. We have developed an algorithm of the transfer-matrix type[33] with which computation of ρ takes only $\sim N_s^2$ steps allowing us to treat very large samples, which is essential to reduce the statistical uncertainty. The method is based on the observation that it is possible to compute directly the four required blocks of G of dimension $\sqrt{N_s}\times\sqrt{N_s}$ that enter in Eq. (8) without ever having to consider the full matrix.

To see this, we write the equation for G, $M\cdot G=1$, in block form:

$$A^n G^{n,n'}-B^{n,n+1}G^{n+1,n'}-B^{n,n-1}G^{n-1,n'}=I\delta_{n,n'} , \tag{9}$$

where the $(N+1)\times(N+1)$ matrices A and B are

$$\begin{aligned} A_{i,j}^n=&\delta_{i,j}\sum_k S^2 J_{i,j}^{n,n}\cos(\theta_i^{0n}-\theta_k^{0n}) \\ &-S^2 J_{i,i+1}^{n,n}\cos(\theta_i^{0n}-\theta_{i+1}^{0n})\delta_{j,i+1} \\ &-S^2 J_{i,i-1}^{n,n}\cos(\theta_i^{0n}-\theta_{i-1}^{0n})\delta_{j,i-1} , \\ B_{i,j}^{n,n\pm1}=&-S^2 J_{i,i}^{n,n\pm1}\cos(\theta_i^{0n}-\theta_i^{0n\pm1})\delta_{i,j} . \end{aligned} \tag{10}$$

Block inversion is performed by introducing transfer matrices, $T^{\pm}$, that propagate G matrices from one column to the columns to its left and to its right, respectively:

$$G^{n_1,n_2}=T_{n_1}^{+}G^{n_1-1,n_2}, \quad n_1>n_2 , \tag{11a}$$

$$G^{n_1,n_2}=T_{n_1}^{-}G^{n_1+1,n_2}, \quad n_1<n_2 . \tag{11b}$$

By iterating Eq. (11a) [(11b)] starting at the left (right) end of the sample, one may relate $\mathbf{G}^{N+1,1}$ and $\mathbf{G}^{1,N+1}$ to $\mathbf{G}^{1,1}$ and $\mathbf{G}^{N+1,N+1}$, respectively. This leads to the following expression for $\mathbf{K}$:

$$\mathbf{K}=[1-T_1^{-}T_2^{-}\cdots T_N^{-}]G^{N+1,N+1} +G^{1,1}[1-T_2^{+}T_3^{+}\cdots T_{N+1}^{+}] . \tag{12}$$

Substituting Eq. (11) into Eq. (9) one may obtain a set of recursion relations satisfied by the transfer matrices as well as explicit expressions for the first and last $G-$ matrix blocks:

$$T_n^{+}=[A^n-B^{n,n+1}T_{n+1}^{+}]^{-1}B^{n,n-1} , \quad T_n^{-}=[A^n-B^{n,n-1}T_{n-1}^{-}]^{-1}B^{n,n+1} , \tag{13a}$$

$$G^{1,1}=[A^1-B^{1,2}T_2^{+}]^{-1} , \quad G^{N+1,N+1}=[A^{N+1}-B^{N+1,N}T_N^{-}]^{-1} . \tag{13b}$$

Equation (12) is evaluated by solving iteratively (13a), multiplying sequentially the transfer matrices as they are obtained, and using the expressions (13b) for the end matrices. Inversion of $\mathbf{K}$ and use of Eq. (7) yields the stiffness constant.

We have applied this formalism to determine the dependence of ρ and c upon x and λ. The input for the present calculations, as well as for those to be described in the next section, are the equilibrium states $\{\theta_i^0\}$ for systems of 20×20, 40×40, and 80×80 spins that we obtained in a previous paper.[7] For each point in the λ-x plane and for each of five different realizations of the random bond distribution, we have ground-state manifolds that consist of 5–20 spin configurations whose energies differ by less than 10^{-5} J/spin. All our data are averaged over the different ground-state ensembles and bond distributions.

Figures 2 and 3 show numerical results for ρ and c for systems of 80×80 spins, and for two values of λ, 0.2, and 0.5. The curves for samples of 20×20 and 40×40 spins are similar except that, for the smaller sizes, ρ is slightly higher and the error bars are much larger. At low concentrations, the stiffness constant and the spin-wave velocity decrease very rapidly with x. Upon entering the spin-glass region, they level off and saturate at a value that decreases when λ does.

There is an exact relationship between the values of the stiffness constant at low and high concentrations that follows from the symmetry properties of the Hamiltonian:

$$\rho(\lambda,x)=\lambda\rho\left[\frac{1}{\lambda},1-x\right] . \tag{14}$$

This relationship implies that $\rho(\lambda,x=0.5)\sim\sqrt{\lambda}$; thus, ρ first vanishes at the point $x=\frac{1}{2}$, $\lambda=0$, where the magnetic system is at its percolation threshold. It is clear that it remains zero in the region $\lambda=0$, $x>\frac{1}{2}$ below percolation. Everywhere else, the stiffness constant is nonzero. Moreover, ρ and c are analytic functions of x at the boundary between the mixed and spin-glass phases. This behavior is in contrast with that of the defect energy, E_d, studied by other authors.[20,21,34,35] The latter quantity is the energy difference between the ground states with periodic and antiperiodic boundary conditions and, therefore, it does not correspond to an adiabatic perturbation. E_d is sensitive to the phase transition and it vanishes nonanalytically as one approaches the critical line, $x_c(\lambda)$. Whereas the finiteness of ρ is a necessary condition for the existence of low-energy spin waves, there is no relationship between E_d and the long-wavelength dynamics of the system.

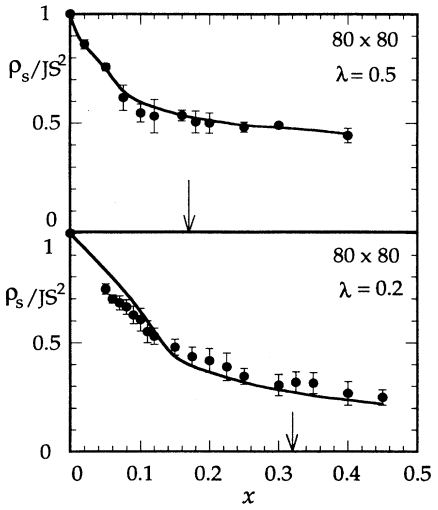

FIG. 2. Spin-wave stiffness vs concentration for systems of 80×80 spins and two values of λ. The points represent the exact results obtained by the transfer-matrix method in Sec. II. The solid curve is the CPA result discussed in Sec. IV.

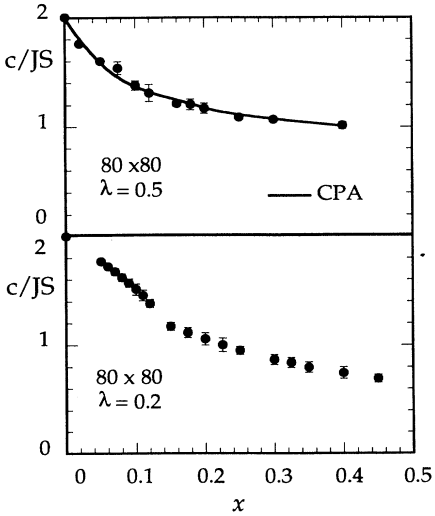

FIG. 3. Spin-wave velocity vs concentration for systems of 80×80 spins and two values of λ. The points represent the exact results obtained by the transfer-matrix method in Sec. II. The solid curve is the CPA result discussed in Sec. IV.

III. THE STRUCTURE FACTOR

To determine the full spectrum of magnetic fluctuations we must construct and diagonalize a spin-wave Hamiltonian. Since the classical ground-state configurations are noncollinear, magnetic excitations are defined relative to a direction that changes from site to site. Several procedures have been developed to generalize ordinary spin-wave theory to this situation.[19,22–25,36,37] In the present case, where the ground-state configuration is planar, a simpler method is available. One proceeds in two stages: first, a nonuniform spin rotation about the z axis is performed such that, in the new system of reference, the expectation values of all the spins point in the x direction (say). Next, the transformed spins are subject to an ordinary spin-wave expansion. As a result of the rotation $\mathbf{S}_i \rightarrow R_3(\theta_i^0)\mathbf{S}_i'$ the exchange constants are renormalized, and the Hamiltonian acquires a new term that couples the gradient of the rotation angle to the spin current:

$$H = -\sum_{\langle ij \rangle} J_{ij}\cos(\theta_i^0-\theta_j^0)(S_i'^x S_j'^x + S_i'^y S_j'^y) - \sum_{\langle ij \rangle} J_{ij}\sin(\theta_i^0-\theta_j^0)(S_i'^x S_j'^y - S_i'^y S_j'^x) \ . \tag{15}$$

We construct the spin-wave Hamiltonian by applying the usual Holstein-Primakoff transformation to Eq. (15). To lowest order in a $1/S$ expansion we have

$$S_i'^x = S - a_i^\dagger a_i \ ,$$

$$S_i'^y \approx \sqrt{S/2}(a_i + a_i^\dagger) \equiv \sqrt{S\lambda_i}\,Q_i \ , \tag{16}$$

$$S_i'^z \approx i\sqrt{S/2}(a_i - a_i^\dagger) \equiv \sqrt{S/\lambda_i}\,P_i \ ,$$

where we have defined appropriate generalized momenta and coordinates, P and Q. In terms of these, the spin-wave Hamiltonian may be written in the form

$$H = -\tfrac{1}{2}S(S+1)\sum_i \lambda_i + \tfrac{1}{2}S\sum_i (P_i^2) + \frac{1}{2S}\sum_{i,j} D_{i,j}Q_iQ_j \ , \tag{17}$$

where

$$D_{i,j} = S^2\sqrt{\lambda_i}\,M_{i,j}\sqrt{\lambda_j} \tag{18}$$

is the dynamical matrix of the problem. It is straightforward to diagonalize (17) and to compute the structure factor in the rotated frame in terms of the eigenvalues and the eigenvectors of D. Transforming the result back to the laboratory frame one obtains the physical structure factor, $S(\mathbf{q},\omega)$. We give here the final results, leaving the details of the calculation for Appendix A.

The structure factor has three components, one elastic and two inelastic, the latter ones representing in- and out-of-plane spin fluctuations. They are given by

$$S^e(\mathbf{q},\omega) = \frac{\pi}{N}\delta(\omega)\left\{\left|\sum_i (S - \langle a_i^\dagger a_i\rangle)e^{i(\theta_i^0 - \mathbf{qR}_i)}\right|^2 + \left|\sum_i (S - \langle a_i^\dagger a_i\rangle)e^{i(\theta_i^0 + \mathbf{qR}_i)}\right|^2\right\} , \tag{19a}$$

$$S^{\mathrm{op}}(\mathbf{q},\omega) = \frac{\pi S}{N}\sum_\alpha \omega_\alpha\delta(\omega-\omega_\alpha)\left|\sum_i \frac{u_i^\alpha}{\sqrt{S\lambda_i}}e^{-i\mathbf{qR}_i}\right|^2 , \tag{19b}$$

$$S^{\mathrm{ip}}(\mathbf{q},\omega) = \frac{\pi S}{2N}\sum_\alpha \frac{\delta(\omega-\omega_\alpha)}{\omega_\alpha}\left\{\left|\sum_i u_i^\alpha\sqrt{S\lambda_i}e^{i(\theta_1^0 - \mathbf{qR}_i)}\right|^2 + \left|\sum_i u_i^\alpha\sqrt{S\lambda_i}e^{i(\theta_i^0 + \mathbf{qR}_i)}\right|^2\right\} , \tag{19c}$$

where ω_α^2 are the eigenvalues of the (positive-definite) dynamical matrix, and u_i^α are the corresponding eigenvectors. Of these three contributions, only the first and the last ones reflect the change of the system of reference. For this reason the structure factors of in-plane and out-of-plane fluctuations are essentially different as will be seen below.

Diagonalization of the dynamical matrix and subsequent evaluation of Eqs. (19) is extremely time consuming. Therefore, we restricted our numerical calculations to systems of a single size, 40×40 spins, and only one value of $\lambda = 0.5$. In Ref. 11 we have calculated the elastic term in Eq. (19) in the classical limit, i.e., without consideration of the quantum reduction of the magnetic moment, $\langle a^\dagger a\rangle$. Computation of this factor for the XY system has shown that here, in contrast with the case of the isotropic model, the effect of quantum fluctuations is very small. In the worst possible case, corresponding to a spin $S = \frac{1}{2}$ and to a concentration of impurities right at the phase transition boundary, the quantum correction amounts to only 16% of the value of the moment and it decreases rapidly as one moves away from the critical point. We thus conclude that the elastic peak is correctly described by the classical calculation[7] and we shall discuss it no more here. The rest of this section is devoted to a description of the dynamic components of $S(\mathbf{q},\omega)$.

Figure 4 shows the structure factor of out-of-plane excitations for four values of the wave vector, and three impurity concentrations, in the mixed phase (a), near the phase boundary (b), and in the spin-glass phase (c), respectively. $S^{\mathrm{op}}(\mathbf{q},\omega)$ shows peaks that are the remnants of the sharp spin waves of the pure system. The peak positions shift to the left and broaden with decreasing x, but out-of-plane excitations remain propagative irrespective of the strength of the disorder. Outside from the wings, the peaks in the figure can be rather well fitted by Lorentzians. The advantage of making such fits is that using them one may extract dispersion relations and widths from the numerical data. Figure 5 shows the dispersion relations thus obtained as a function of impuri-

ty concentration. One can distinguish two regimes. In the mixed phase, the dispersion curve flattens at small q as a consequence of softening, but, with increasing q, it turns upwards to approach the curve corresponding to the pure system. On the spin-glass side of the phase diagram this does not happen, and the excitation energies are strongly renormalized at all wave vectors. The reason for this difference is that in the mixed phase there exist large ferromagnetic domains whose typical size, ξ, depends upon the concentration of impurities. Out-of-plane excitations of wavelength shorter than ξ propagate almost freely in the interior of these domains where the environment is similar to that in the pure system; then their dispersion relation stays close to the unperturbed one. On the spin-glass side of the transition, the ferromagnetic domains are always of microscopic size and this mechanism cannot come into play.

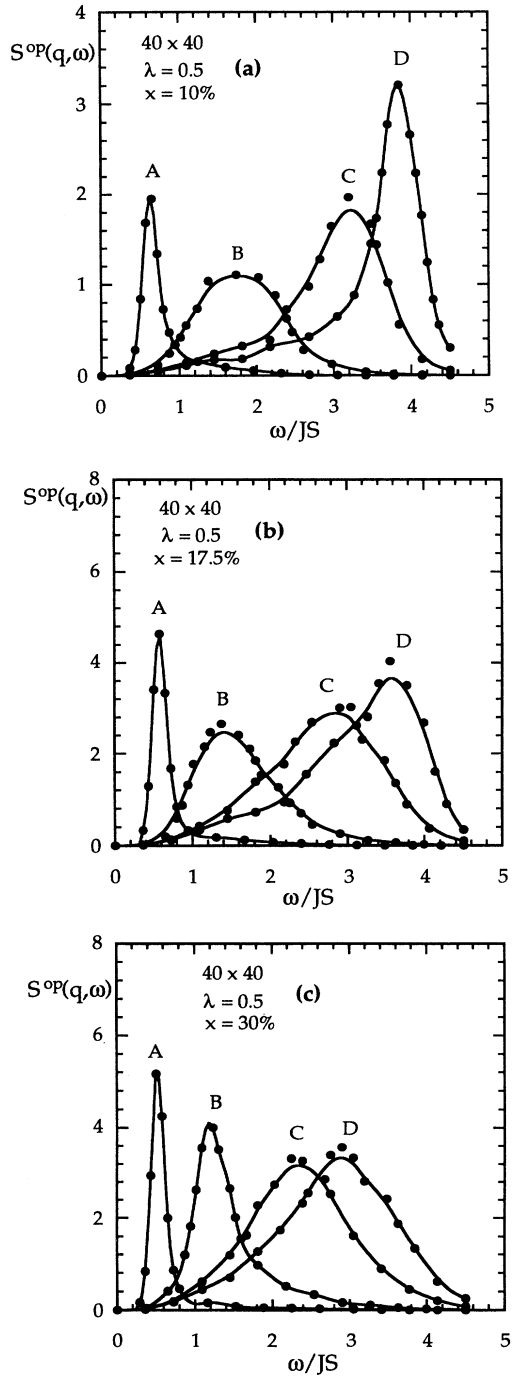

FIG. 4. Dynamic structure factor of the out-of-plane fluctuations for systems of 40×40 spins, $\lambda=0.5$, and three concentrations, (a) $x=10\%$, (b) $x=17.5\%$, and (c) $x=30\%$. Spectra are shown for four values of $|\mathbf{q}|$: (A), $3\pi/20$, (B) $7\pi/20$, (C) $13\pi/20$, and (D) π, respectively. The solid lines are the fits discussed in the text.

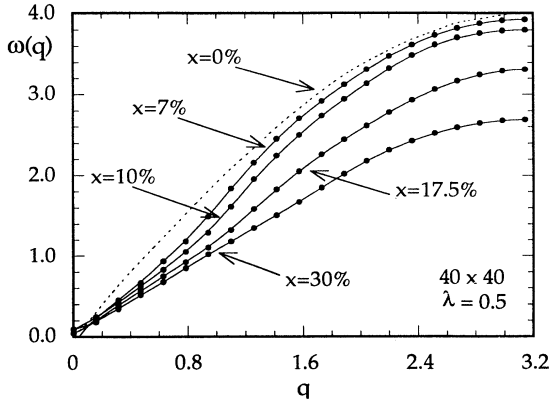

FIG. 5. Dispersion relations for out-of-plane spin waves for systems of 40×40 spins and $\lambda=0.5$ as a function of impurity concentration.

It may be seen by inspection of Fig. 4 that the intensities and the widths of the spin-wave peaks show pronounced variations as functions of q and x. This is shown quantitatively in Fig. 6 where we represent the peak widths, Γ, as a function of the peak positions. In the spin-glass phase, Γ increases with the energy of the excitations. In contrast, in the mixed phase, there is a crossover at a wave vector $q \approx \xi^{-1}$ to a regime where the

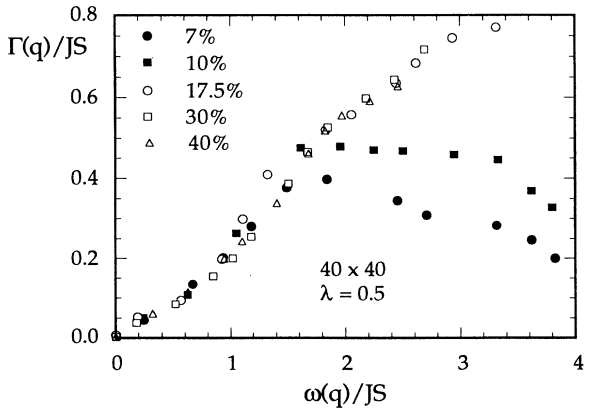

FIG. 6. Spin-wave width as a function of spin-wave energy for systems of 40×40 spins and $\lambda=0.5$, as a function of impurity concentration.

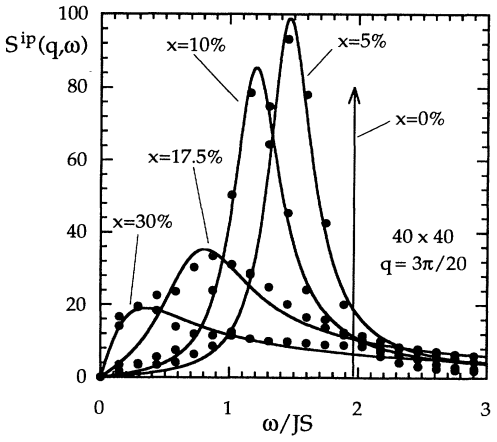

FIG. 7. Dynamic structure factor of the in-plane fluctuations for systems of 40×40 spins, $\lambda=0.5$, and four different concentrations. The curves shown correspond to a single value of $|\mathbf{q}|=3\pi/20$.

width levels off and then decreases. Whatever the concentration, the width vanishes as $\omega\to0$. In their study of the three-dimensional Edwards-Anderson model, Huber and Ching[24,25,38] have found that, at low frequency, $\Gamma\alpha\omega^2$. Our results are consistent with $\Gamma\alpha\omega^{1+\Delta}$, with $0<\Delta<1$, but we do not have enough data to determine precisely the value of Δ.

A striking feature of Fig. 6 is that, within our numerical uncertainty, all data points pertaining to the disordered phase (and to the mixed phase before the crossover) sit on the same universal curve meaning that the linewidth depends on the strength of the disorder only through the excitation frequency, $\omega(q)$. This explains why some of the peaks in Fig. 4 become *narrower* when the disorder increases: the energy of the excitation decreases for a larger value of x and this leads to a smaller width.

The dynamic structure factor of the in-plane excitations, $S^{ip}(\mathbf{q},\omega)$, is shown in Fig. 7 for a fixed value of q and several impurity concentrations. The line shapes are in this case qualitatively different from those that we just discussed and, with increasing x, they evolve from an inelastic to a quasielastic profile. The reason for this evolution is that the linewidth of in-plane excitations is determined not just by the intrinsic effects of randomness but also by the convolution that relates the correlation function in the rotated frame to that in the laboratory frame. This last effect is a source of inhomogeneous broadening and it produces non-Lorentzian line shapes. When $\omega\to0$ the intrinsic component of the width vanishes but the inhomogeneous component becomes energy independent. As a result, low-energy excitations always exhibit a diffusive line shape.

IV. COHERENT POTENTIAL APPROXIMATION

For large samples, the calculations presented in the previous sections are very demanding in computer time. It is therefore of interest to investigate whether our numerical results can be reproduced with good accuracy by an approximate analytical theory that would be easier to implement than the exact numerical methods described above.

The coherent potential approximation is a convenient framework for the treatment of the effects of disorder on magnetic excitations and it has been used in the past to study spin waves in disordered isotropic spin models.[7,27,29] To our knowledge, it has never been applied to the case of the planar system which turns out to be much more involved. The starting point for the analysis is the Hamiltonian of Eq. (15), in the spin-wave representation,

$$H_{SW}=S\sum_i\lambda_i a_i^\dagger a_i-\frac{S}{4}\sum_{i,j}\tilde{J}_{i,j}(a_i^\dagger+a_i)(a_j^\dagger+a_j)\ . \tag{20}$$

The structure of Eq. (20) implies the existence of both normal and anomalous boson propagators. Because of this feature, treatment of the XY model is considerably more complicated than that of the isotropic model. The boson Green's function is now the 2×2 matrix:

$$G_{ij}(t)=\begin{bmatrix}\langle\langle a_i(t)|a_j^\dagger\rangle\rangle & \langle\langle a_i(t)|a_j\rangle\rangle\\ \langle\langle a_i^\dagger(t)|a_j^\dagger\rangle\rangle & \langle\langle a_i^\dagger(t)|a_j\rangle\rangle\end{bmatrix}, \tag{21}$$

where $\langle\langle A(t)|B\rangle\rangle=-i\theta(t)\langle[A(t),B]\rangle$ denotes the usual retarded Green's function. The in- and out-of-plane components of the dynamic structure factor are given by averages over the distribution of impurities of various combinations of elements of the matrix of Eq. (21):

$$\begin{aligned}S^{ip}(\mathbf{q},\omega)&=S\sum_{\alpha,\beta}\mathrm{Im}\{G^{\alpha,\beta}_{\mathbf{q},\mathbf{q}}(\omega-i\eta)\}_{av}]\ ,\\ S^{op}(\mathbf{q},\omega)&=S\sum_{\alpha,\beta}(-1)^{\alpha+\beta}\mathrm{Im}[\{G^{\alpha,\beta}_{\mathbf{q},\mathbf{q}}(\omega-i\eta)\}_{av}]\ .\end{aligned} \tag{22}$$

The frequency-dependent effective medium is defined such that the translationally invariant *averaged* Green's function of the nonuniform system with the Hamiltonian of Eq. (20) is the same as the Green's function of a uniform system described by the effective Hamiltonian

$$\begin{aligned}H_{eff}(\omega)=S\sum_{\mathbf{q}}\{&A(\mathbf{q},\omega)a_{\mathbf{q}}^\dagger a_{\mathbf{q}}\\ &-\tfrac{1}{2}[B(\mathbf{q},\omega)a_{\mathbf{q}}^\dagger a_{-\mathbf{q}}^\dagger\\ &+B^*(-\mathbf{q},-\omega)a_{\mathbf{q}}a_{-\mathbf{q}}^\dagger]\}\ .\end{aligned} \tag{23}$$

In other words, we require that

$$G_{av}(\mathbf{q},\omega)=\begin{bmatrix}\omega-A(\mathbf{q},\omega) & B(\mathbf{q},\omega)\\ B^*(-\mathbf{q},-\omega) & -\omega-A(\mathbf{q},-\omega)\end{bmatrix}^{-1}\ . \tag{24}$$

As in the case of the more familiar scalar problem we introduce a T matrix to relate the exact and averaged Green's function:[7,27,29]

$$\begin{aligned}G(\mathbf{q},\mathbf{q}',\omega)=&G_{av}(\mathbf{q},\omega)\delta_{\mathbf{q},\mathbf{q}'}\\ &+G_{av}(\mathbf{q},\omega)T(\mathbf{q},\mathbf{q}',\omega)G_{av}(\mathbf{q}',\omega)\ .\end{aligned} \tag{25}$$

T satisfies the equation

$$\begin{aligned}T(\mathbf{q},\mathbf{q}',\omega)=&(H-H_{eff})_{\mathbf{q},\mathbf{q}'}\\ &+\sum_{\mathbf{p}}(H-H_{eff})_{\mathbf{q},\mathbf{p}}G_{av}(\mathbf{p},\omega)T(\mathbf{p},\mathbf{q}',\omega)\ .\end{aligned} \tag{26}$$

By averaging Eq. (25) we obtain the condition

$$\{T(\mathbf{q},\mathbf{q}',\omega)\}_{\mathrm{av}} \equiv T_{\mathrm{av}}(\mathbf{q},\omega)\delta_{\mathbf{q},\mathbf{q}'}=0 \tag{27}$$

that, used in conjunction with Eq. (26), determines implicitly the parameters of the effective Hamiltonian.

The system of equations (25)–(27) is formally exact but cannot be solved for a general form of the effective Hamiltonian. In order to proceed further, we shall make two approximations. The first one is an *ansatz* on the form of H_{eff}: we shall assume that the effective medium is appropriately described by local and first-neighbor interactions. This leads to the parametrization

$$\begin{aligned} A(\mathbf{q},\omega)&=4SJ[a_0(\omega)-\gamma(\mathbf{q})a_1(\omega)]\ , \\ B(\mathbf{q},\omega)&=4SJ[b_0(\omega)-\gamma(\mathbf{q})b_1(\omega)]\ , \end{aligned} \tag{28}$$

where $\gamma(\mathbf{q})=\frac{1}{2}[\cos(q_x a)+\cos(q_y a)]$. This important assumption implies that the potential $H-H_{\mathrm{eff}}$ of Eq. (26) can be written as a sum of terms, each of which refers to a bond. The second approximation is the standard CPA which states that in the evaluation of the averaged T matrix from Eqs. (26) and (27) one may neglect the interference between multiply scattered waves that originate from *different* bonds. Granted these two assumptions, a lengthy but otherwise straightforward calculation yields

$$\begin{aligned} T_{\mathrm{av}}(\mathbf{q},\omega)=&([1-\gamma(\mathbf{q})][V^0(\omega)-V^1(\omega)]\{1-[\Phi^0(\omega)-\Phi^1(\omega)][V^0(\omega)-V^1(\omega)]\}^{-1} \\ &+[1+\gamma(\mathbf{q})][V^0(\omega)+V^1(\omega)]\{1-[\Phi^0(\omega)+\Phi^1(\omega)][V^0(\omega)+V^1(\omega)]\}^{-1})_{\mathrm{av}}=0\ , \end{aligned} \tag{29}$$

where

$$\{\cdots\}_{\mathrm{av}}=\int\{\cdots\}P(\tilde{J})d\tilde{J}\ . \tag{30}$$

In the above, $P(\tilde{J})$ is the distribution of the renormalized exchange constants [cf. Eq. (17)], and

$$\begin{aligned} \Phi^0(\omega)&=\frac{1}{N_s}\sum_{\mathbf{q}}G_{\mathrm{av}}(\mathbf{q},\omega)\ , \\ \Phi^1(\omega)&=\frac{1}{N_s}\sum_{\mathbf{q}}\gamma(\mathbf{q})G_{\mathrm{av}}(\mathbf{q},\omega)\ , \\ V^0(\omega)&=S\begin{bmatrix}\tilde{J}-a_0(\omega) & b_0(\omega)\\ b_0(\omega) & \tilde{J}-a_0(-\omega)\end{bmatrix}\ , \\ V^1(\omega)&=-S\begin{bmatrix}\frac{\tilde{J}}{2}-a_1(\omega) & \frac{\tilde{J}}{2}+b_1(\omega)\\ \frac{\tilde{J}}{2}+b_1(\omega) & \frac{\tilde{J}}{2}-a_1(-\omega)\end{bmatrix}\ . \end{aligned} \tag{31}$$

Notice that the T matrix of Eq. (29) contains only in-site and nearest-neighbor interactions. This shows that our assumption concerning the spatial structure of the effective Hamiltonian is consistent with the CPA.

For a fixed frequency Eqs. (24), (29), and (30) form a closed system of equations for the four complex parameters $a_\alpha(\omega)$ and $b_\alpha(\omega)$, $\alpha=0,1$. The numerical solution of these equations would hardly be possible were it not for the fact that it is possible to derive analytic expressions for the functions Φ^0 and Φ^1 that appear in Eq. (29) in terms of combinations of complete elliptic integrals of the first kind of complex argument, just as in the pure case.[39] In the rest of this section we describe the properties of the solutions. The interested reader will find some technical details on the solution of the CPA equations in Appendix B.

We have solved the CPA equations for $\lambda=0.5$ and various concentrations. As an example, we plot in Fig. 8 the effective couplings as a function of frequency for $x=10\%$. In the presence of disorder, they depart considerably from the values they take in the pure system, $a_0(\omega)=1$, $a_1(\omega)=-b_1(\omega)=\frac{1}{2}$, $b_0(\omega)=0$, particularly at low frequency. A surprising feature of Fig. 8(a) is that the ratio of the real parts of the diagonal couplings, $a_0(\omega)/a_1(\omega)$, is very close to 2, the unperturbed value, despite the fact that, separately, they depend rather strongly upon frequency. The imaginary parts of these couplings are almost identical throughout the spectrum.

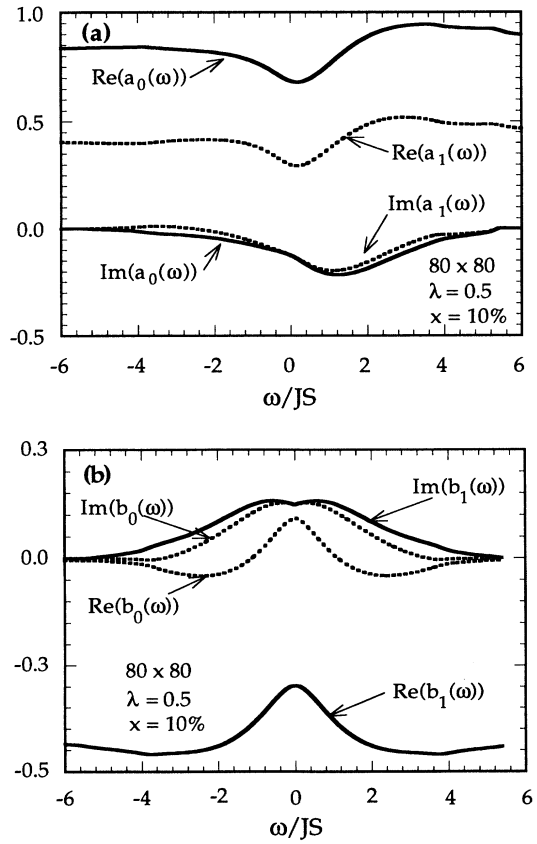

FIG. 8. Frequency dependence of the real and imaginary parts of the effective couplings of the CPA Hamiltonian. (a) normal terms, (b) anomalous terms.

A first test of the quality of the CPA is its ability to reproduce the low-energy results of Sec. II. Applying to the CPA response functions the hydrodynamic relations

$$\frac{1}{\rho} = -\lim_{q\to 0} q^2 \lim_{\omega\to 0} \mathrm{Re}\{G^{\mathrm{ip}}(\mathbf{q},\omega)\} ,$$
$$\chi_\perp = \lim_{q\to 0}\lim_{\omega\to 0} \mathrm{Re}\{G^{\mathrm{op}}(\mathbf{q},\omega)\} , \tag{32}$$

one may readily show that

$$\rho_{\mathrm{CPA}} = JS^2 \mathrm{Re}\{a_1(0) - b_1(0)\} ,$$
$$\frac{1}{\chi_{\perp\mathrm{CPA}}} = \frac{8}{J}\mathrm{Re}\{b_0(0) - b_1(0)\} . \tag{33}$$

The results for ρ and c are shown by the solid lines in Figs. 2 and 3 together with the exact values obtained as discussed in Sec. II. The agreement is excellent for the spin-wave velocity and satisfactory for the stiffness constant. In the case of the latter quantity, the result quoted in Eq. (33) is identical to that derived by Vannimenus *et al.*[9] by a different approach provided we replace in their expressions the bare exchange constant by the renormalized one.

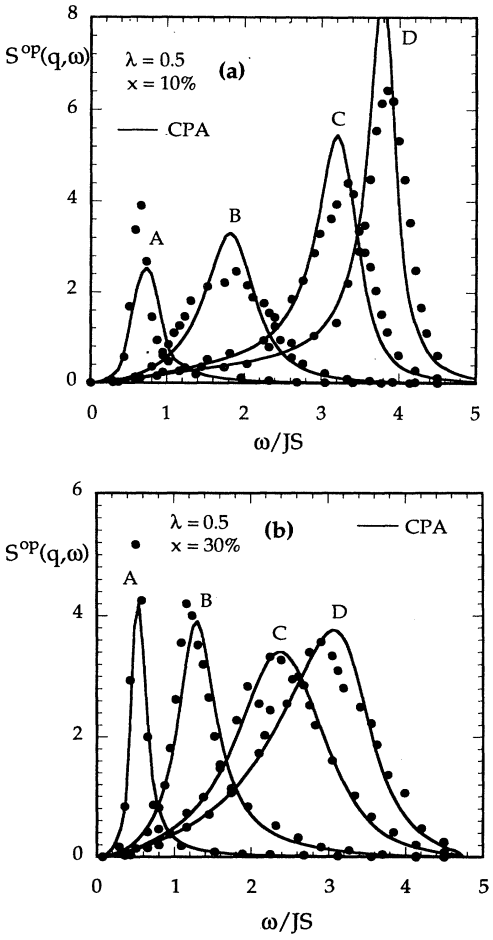

FIG. 9. CPA dynamic structure factor of out-of-plane fluctuations for $\lambda = 0.5$, and two concentrations, (a) $x = 10\%$, and (b) $x = 30\%$. The data points are the exact results of Figs. 4(a) and 4(c). The solid lines are the CPA results.

The CPA not only reproduces remarkably well the exact results in the hydrodynamic region but it also gives a correct overall picture of the full excitation spectrum. We computed the CPA dynamic structure factor for two concentrations, 10 and 30%. Figures 9(a) and 9(b), where we plot the results for the out-of-plane component of $S(\mathbf{q},\omega)$, show that the approximation predicts quite well the positions and the widths of the spin-wave peaks. The agreement is less satisfactory in the case of the in-plane component because of the CPA's failure to describe correctly the behavior of $S^{\mathrm{ip}}(\mathbf{q},\omega)$ as $\omega\to 0$, a problem that has also been noticed by other authors.[40,41]

The determination of the effective Hamiltonian by a self-consistent solution of Eqs. (29) and (30) is certainly a nontrivial task. However, the computer time and memory requirements of the CPA calculation are much less stringent than those of the diagonalizations of the previous section. The quality of the results furnished by this method suggest that it is a good alternative to the exact methods when one is interested in the overall features of the excitation spectrum. For comparison, we have also performed approximate calculations with two other methods, straightforward lowest-order perturbation theory and the average T-matrix approximation. Except for the lowest concentrations, the results of these two approaches differ considerably from both the exact and the CPA results.

V. CONCLUSIONS

In this paper we have studied numerically and analytically a random 2D XY model whose spin dynamics is found to be qualitatively similar to that of the high-T_c oxides in their insulating phase. The stiffness constant and the spin-wave velocity are very sensitive to the presence of impurities, in agreement with experimental observation. Both quantities decrease rapidly when the concentration of impurities, x, increases and are finite in the spin-glass phase as expected on general grounds.[19] The features of the spin-wave dynamics of the system depend strongly on the polarization of the fluctuations. In-plane fluctuations are inhomogeneously broadened and become overdamped when disorder increases, whereas out-of-plane ones, though broadened and shifted to smaller energies, always remain propagative, a behavior that has been seen experimentally in $YBa_2Cu_3O_{6+\delta}$. The linewidths exhibit an interesting frequency dependence that is different in the mixed and spin-glass phases. The coherent potential approximation developed here gives results that are in remarkable agreement with those of the exact methods, suggesting that the CPA is a good alternative to the heavy numerical calculations required by the latter.

We have not discussed in this work the quantum corrections to the stiffness constant[42,43] and the spin-wave velocity. The effects of quantum fluctuations are known to be very important in the case of the 2D isotropic Heisenberg antiferromagnet where, even in the pure case, the quantum reduction of the sublattice magnetization is very large.[44,45] It has been suggested that, in this system, in the presence of frustration, zero-point fluctuations may be strong enough to destroy long-range order. In the

case of the pure XY model, quantum effects are much smaller. Our calculations for $\lambda=0.5$ indicate that, for this value of the coupling, they are also small in the disordered case. We cannot exclude a quantum transition to a state with no long-range order for smaller values of λ. This issue is under current investigation.

APPENDIX A

In this appendix we derive Eqs. (19a)–(19c) for the dynamic structure factor. In the transformed frame, the nonvanishing correlation functions are, in the spin-wave approximation,

$$\langle S_i'^x(t)S_j'^x(0)\rangle \approx \langle S-a_i^\dagger a_i\rangle\langle S-a_j^\dagger a_j\rangle \ , \tag{A1}$$

$$\langle S_i'^y(t)S_j'^y(0)\rangle \approx S\sqrt{\lambda_i\lambda_j}\langle Q_i(t)Q_j(0)\rangle \ , \tag{A2}$$

$$\langle S_i'^z(t)S_j'^z(0)\rangle \approx \frac{S}{\sqrt{\lambda_i\lambda_j}}\langle P_i(t)P_j(0)\rangle \ , \tag{A3}$$

where Q_i and P_i are the generalized coordinates and momenta defined in Eq. (16). The dynamical matrix D is symmetric and positive definite. Thus, it has real, positive, eigenvalues and real eigenvectors. We write

$$\sum_j D_{i,j}u_j^\alpha=\omega_\alpha^2 u_i^\alpha \ . \tag{A4}$$

It follows from Eqs. (A4) and (17) that the Hamiltonian may be diagonalized by the transformation

$$\begin{aligned} Q_i&=\sum_\alpha \frac{u_i^\alpha}{\sqrt{2\omega_\alpha}}(\beta_\alpha+\beta_\alpha^\dagger) \ , \\ P_i&=i\sum_\alpha u_i^\alpha\sqrt{\omega_\alpha/2}(\beta_\alpha-\beta_\alpha^\dagger) \ , \end{aligned} \tag{A5}$$

where β ($\beta^\dagger$) are boson annihilation (creation) operators. The diagonal Hamiltonian is

$$H=-\tfrac{1}{2}S(S+1)\sum_i\lambda_i+\sum_\alpha\omega_\alpha(\beta_\alpha^\dagger\beta_\alpha+\tfrac{1}{2}) \ . \tag{A6}$$

Substituting (A5) into (A1) and using the fact that there are no excitations in the ground state of (A6) we obtain

$$\langle S_i'^z S_j'^z\rangle_\omega \approx \frac{2\pi S}{\sqrt{\lambda_i\lambda_j}}\sum_\alpha u_i^\alpha u_j^\alpha\frac{\omega_\alpha}{2}\delta(\omega-\omega_\alpha) \ , \tag{A7a}$$

$$\langle S_i'^y S_j'^y\rangle_\omega \approx 2\pi S\sqrt{\lambda_i\lambda_j}\sum_\alpha\frac{u_i^\alpha u_j^\alpha}{2\omega_\alpha}\delta(\omega-\omega_\alpha) \ . \tag{A7b}$$

The out-of-plane component z is not modified by the rotation. The in-plane component, on the other hand, must be transformed back to the laboratory frame. We have

$$\begin{aligned} S^{\rm ip}(\mathbf{q},\omega)&=\frac{1}{N}\sum_{i,j}e^{i\mathbf{q}\cdot(\mathbf{R}_i-\mathbf{R}_j)}\cos(\theta_i^0-\theta_j^0)\langle S_i'^y S_j'^y\rangle_\omega \ , \\ S^{\rm op}(\mathbf{q},\omega)&=\frac{1}{N}\sum_{i,j}e^{i\mathbf{q}\cdot(\mathbf{R}_i-\mathbf{R}_j)}\langle S_i'^z S_j'^z\rangle_\omega \ . \end{aligned} \tag{A8}$$

Substitution of (A7) into (A8) leads to Eqs. (19b) and (19c). The elastic contribution may be treated in a similar way.

APPENDIX B

For fixed frequency, the T matrix of Eq. (29) contains four complex elements of which only three are independent. The solution of the CPA system of equations, (24) and (28)–(31), reduces to the simultaneous solution of 12 nonlinear equations with 12 unknowns, the real and imaginary parts of $a_\alpha(\pm\omega)$ and $b_\alpha(\omega)$, $\alpha=0,1$. One feature that makes the problem solvable despite its formidable appearance is that the two moments of the $G_{\rm av}$ matrix that appear in Eq. (30), $\Phi^{(0,1)}(\omega)$, may be evaluated analytically. Indeed, it follows from Eqs. (24), (28), and (31) that all the required matrix elements can be expressed in terms of

$$I_n=\frac{1}{N}\sum_{\mathbf{k}}\frac{\gamma(\mathbf{k})^n}{\Delta(\mathbf{k},\omega)}, \quad n=0,1,2 \ , \tag{B1}$$

where $\Delta(\mathbf{k},\omega)$ is the determinant of the matrix of Eq. (24). Using Eq. (28) we find

$$I_n=\frac{1}{N}\sum_{\mathbf{k}}\frac{\gamma(\mathbf{k})^n}{u(\omega)\gamma(\mathbf{k})^2+v(\omega)\gamma(\mathbf{k})+w(\omega)} \ , \tag{B2}$$

where the functions u, v, and w are determined by the couplings a_α and b_α. By decomposing the denominator in Eq. (B2) in simple fractions, we can express all the I_n in terms of combinations of integrals of the form

$$I_n^0=\frac{1}{N}\sum_{\mathbf{k}}\frac{\gamma(\mathbf{k})^n}{z_1(\omega)-z_2(\omega)\gamma(\mathbf{k})} \tag{B3}$$

with z_1 and z_2 complex functions of ω. These integrals have been evaluated by Morita.[39] The result is

$$\begin{aligned} I_0^0(z_1,z_2)&=\frac{2}{\pi z_1}K\left[\frac{z_2}{z_1}\right] \ , \\ I_1^0(z_1,z_2)&=\frac{1}{z_2}\left[\frac{2}{\pi}K\left[\frac{z_2}{z_1}\right]-1\right] \ , \\ I_2^0(z_1,z_2)&=\frac{z_1}{z_2^{\,2}}\left[\frac{2}{\pi}K\left[\frac{z_2}{z_1}\right]-1\right] \ , \end{aligned} \tag{B4}$$

where K denotes the complete elliptic integral of the first kind of complex argument. A very fast algorithm to compute the elliptic functions is based on the following recurrence relations.[46] Let

$$a_0=1, \quad b_0=\sqrt{1-z^2} \tag{B5}$$

and, for $n\geq 1$,

$$a_n=\tfrac{1}{2}(a_{n-1}+b_{n-1}), \quad b_n=\sqrt{a_{n-1}b_{n-1}} \ , \tag{B6}$$

then,

$$K(z)=\lim_{N\to\infty}\frac{\pi}{2a_N} \ . \tag{B7}$$

An approximation to K can thus be obtained by evaluating the right-hand side of (B7) at some large value of N rather than taking the limit. In practice, it is sufficient to take $N<50$ to obtain an accuracy better than a part in 10^8 in K.

Since, to our surprise, we could not find in standard books on numerical methods any algorithm to solve a system of simultaneous nonlinear equations that did not require knowledge of the partial derivatives of the functions, it may be worth presenting here a simple method that we developed to solve the CPA equations but that is quite general. It is, in fact, a multidimensional generalization of the secant method usually employed to find the zeroes of a single function.

Let the system of equations to be solved be

$$f_i(x_1,x_2,\ldots,x_N)=0, \quad i=1,2,\ldots,N \ . \tag{B8}$$

Let $x^{(0)}$ and $x^{(-1)}$ be two points in the N-dimensional space of the variables. Define the following sequence ($n \geq 0$):

$$x_i^{(n+1)}=x_i^{(n)}-\sum_j L_{i,j}^{-1}(x^{(n)},x^{(n-1)})f_j(x^{(n)}) \ , \tag{B9}$$

where the matrix L has elements

$$L_{i,j}(x^{(n)},x^{(n-1)})=\frac{f_i(x_1^{(n)},\ldots,x_j^{(n)},\ldots,x_N^{(n)})-f_i(x_1^{(n)},\ldots,x_j^{(n-1)},\ldots,x_N^{(n)})}{x_j^{(n)}-x_j^{(n-1)}} \ . \tag{B10}$$

It can easily be shown that, if the sequence (B9) converges, it does so to a point x^* that is a solution of the system (B8). Moreover, convergence is quadratic, i.e., the error in the determination of x at the $(n+1)$-th stage is proportional to the square of that at the nth stage.

[1]M. Matsuda, K. Yamada, K. Kakurai, T. R. Thurston, Y. Endoh, Y. Hikada, R. J. Birgenau, M. A. Kastner, P. M. Gehring, A. H. Moudden, and G. Shirane, Phys. Rev. B **42**, 10098 (1990).

[2]S. Chakravarty, B. I. Halperin, and D. R. Nelson, Phys. Rev. B **39**, 2344 (1989).

[3]J. Rossat-Mignod, L. P. Regnault, C. Vettier, P. Burlet, J. Y. Henry, and G. Lapertot, Physica B **163**, 4 (1990).

[4]J. Rossat-Mignod, L. P. Regnault, M. J. Jurgens, P. Burlet, J. Y. Henry, and G. Lapertot, in *Dynamics of Magnetic Fluctuations in High-T_c Superconductors,* Vol. 246 of NATO Advanced Study Institute, Series B: Physics, edited by G. Reiter, P. Horsch, and G. C. Psaltakis (Plenum, New York, 1991), p. 35.

[5]A. Aharony, R. J. Birgeneau, A. Coniglio, M. A. Kastner, and M. E. Stanley, Phys. Rev. Lett. **60**, 1330 (1988).

[6]D. Harshman, G. Aeppli, G. P. Espinosa, A. S. Cooper, J. P. Remeika, E. J. Ansaldo, T. M. Riseman, D. L. Williams, B. Ellina, and T. F. Rosenbaum, Phys. Rev. B **38**, 852 (1988).

[7]P. Gawiec and D. R. Grempel, Phys. Rev. B **44**, 2613 (1991).

[8]W. M. Saslow and G. N. Parker, Phys. Rev. B **28**, 11733 (1988).

[9]J. Vannimenus, S. Kirkpatrick, F. D. M. Haldane, and C. Jayaprakash, Phys. Rev. B **39**, 4634 (1989).

[10]W. Y. Ching and D. L. Huber, J. Appl. Phys. **67**, 5743 (1990).

[11]D. L. Huber and W. Y. Ching, Phys. Rev. B **42**, 493 (1990).

[12]W. Brenig and A. P. Kampf, Phys. Rev. B **43**, 12914 (1991).

[13]K. Lee and P. Schlottmann, Phys. Rev. B **42**, 4426 (1990).

[14]D. N. Aristov and S. V. Maleyev, Z. Phys. B **81**, 433 (1990).

[15]N. Bulut, D. Hone, D. J. Scalapino, and E. Y. Loh, Phys. Rev. Lett. **62**, 2192 (1989).

[16]W. Saslow and R. Erwin, Phys. Rev. B **45**, 4759 (1992).

[17]J. Rossat-Mignod, L. P. Regnault, M. J. Jurgens, C. Vettier, P. Burlet, J. Y. Henry, and G. Lapertot, Physica C **162-164**, 1269 (1989).

[18]P. Reed, J. Phys. C **12**, L475 (1979).

[19]B. I. Halperin and W. M. Saslow, Phys. Rev. B **16**, 2154 (1977).

[20]C. L. Henley, Ann. Phys. (N.Y.) **156**, 368 (1984).

[21]M. Cieplak and M. Z. Cieplak, J. Phys. C **18**, 1481 (1985).

[22]L. R. Walker and R. E. Walstedt, Phys. Rev. Lett. **38**, 514 (1977).

[23]L. R. Walker and R. E. Walstedt, Phys. Rev. B **22**, 3816 (1980).

[24]D. L. Huber, W. Y. Ching, and M. Fibich, J. Phys. C **12**, 3535 (1979).

[25]D. L. Huber and W. Y. Ching, J. Phys. C **13**, 5579 (1980).

[26]D. R. Grempel and P. Gawiec, J. Magn. Magn. Mater. **104-107**, 289 (1992).

[27]R. A. Tahir-Kheli, Phys. Rev. B **6**, 2809 (1972).

[28]E.-N. Foo and S. M. Bose, Phys. Rev. B **9**, 347 (1973).

[29]E.-N. Foo and S. M. Bose, Phys. Rev. B **9**, 3944 (1973).

[30]W. M. Saslow and G. N. Parker, Phys. Rev. Lett. **56**, 1074 (1986).

[31]G. N. Parker and W. M. Saslow, Phys. Rev. B **38**, 11718 (1988).

[32]B. I. Halperin and P. C. Hohenberg, Phys. Rev. **188**, 898 (1969).

[33]J. Hori, *Spectral Properties of Disordered Chains and Lattices* (Pergamon, Oxford, 1968).

[34]B. W. Morris, S. G. Colborne, M. A. Moore, A. J. Bray, and J. Canisius, J. Phys. C **19**, 1157 (1986).

[35]A. J. Bray and S. Feng, Phys. Rev. B **36**, 8456 (1987).

[36]S. L. Guinzburg, Zh. Eksp. Teor. Fiz. **75**, 1497 (1978) [Sov. Phys. JETP **48**, 756 (1978)].

[37]W. Saslow, Phys. Rev. B **27**, 6873 (1983).

[38]W. Y. Ching, K. M. Leung, and D. L. Huber, Phys. Rev. Lett. **39**, 729 (1987).

[39]R. Morita, J. Math. Phys. **12**, 1744 (1971).

[40]P. Lloyd and J. Oglesby, J. Phys. C **9**, 4383 (1976).

[41]B. G. Nickel and W. H. Butler, Phys. Rev. Lett. **30**, 373 (1973).

[42]R. R. P. Singh and D. A. Huse, Phys. Rev. B **40**, 7247 (1989).

[43]P. Kopietz and G. Castilla, Phys. Rev. B **43**, 11100 (1991).

[44]T. Aoki, J. Phys. Soc. Jpn. **61**, 2909 (1992).

[45]J. I. Igarashi and A. Watabe, Phys. Rev. B **43**, 13456 (1991).

[46]*Handbook of Mathematical Functions,* edited by M. Abramowitz and I. A. Stegun (Dover, New York, 1964).